Effect of Feeder Configuration on the Microstructure of Ductile Cast Iron

Nikolaj Kjelgaard Vedel-Smith[1], Niels Skat Tiedje[1]

[1]Technical University of Denmark, Department of Mechanical Engineering, Produktionstorvet Building 427A, 2800 Kgs. Lyngby, Denmark

Keywords: SG Iron, Color Etching, Feeder, Porosities, Dimensional Accuracy, Hot spot

Abstract

Feeding and microstructure of a test casting rigged with different feeder combinations was studied. Castings were examined and classified by soundness and microstructure. Subsequently the casting macro- and microstructure was analyzed to study how differences in solidification and segregation influence the soundness of different sections of the castings. Moreover, the microstructural changes due to variations in thermal gradients are classified, and the variations in the mushy zone described.

The paper discusses how solidification and segregation influence porosity and microstructure of ductile iron castings. The goal is to enable metallurgists and foundry engineers to more directly target mushy zone development to prolong the possibility to feed through this section. Keeping smaller section open for an extended period will make it possible to use fewer or smaller feeders, with reduced energy consumption and cheaper products as a result.

Introduction

Energy for melting is a significant expense and represents approx. one quarter of the production cost for cast iron foundries. New applications for ductile iron (DI) increase the requirements for improved mechanical properties, and some of these alloys show significant problems with shrinkage and porosities. Larger modulus feeders and better designs are required to successfully cast sound castings. The changes in alloy composition also entail a different behavior of the primary and secondary graphite expansion making it difficult to feed secluded sections of the casting.

This paper is the result of an ongoing project, involving several companies, working towards characterizing, quantifying and understanding the effect and functioning of various feeder applications.

On vertically parted molds it can be difficult to place feeders freely. Traditional feeders are geometrically restrained to the upper half of the parting line. Spot feeders, on vertically parted molds, enable feeding of secluded sections located away from the parting line. The spot feeders can be insulation, exothermic or a combination, and provide heat and melt to a given section.

Experimental Setup

Casting Geometry

The test geometry used for the experiments consist of a disc with an inner boss and an outer ring, separated by a thin plate like section. The geometry is designed to display the same problems as found in disc brakes, flywheels and other castings with combinations of small and large modulus sections. The casting layout and feeder location is seen in Fig. 1. For more details please refer to [1].

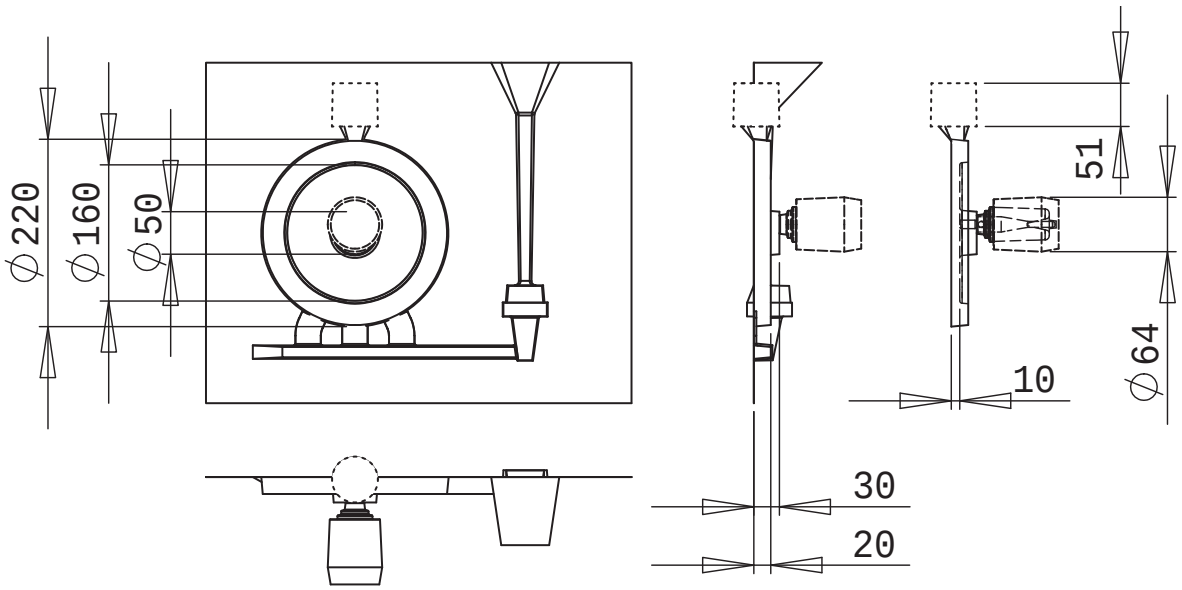

Figure 1: Overview of casting geometry and feeder placement. The dotted lines indicate the top feeder, and the dashed lines indicate the centre feeder. Measurements are in mm.

All feeders used where sleeved and had the same geometric modulus (M_g), calculated as $M_g = \frac{V}{S}$, where V is the volume of the feeder and S is the cooling surface. By changing the sleeve material, the thermal (or true) modulus (M_t) was increased without changing the geometry—thus keeping the ferrostatic pressure constant. The modulus of the feeders change because of the thermal properties of the chosen sleeve material. This multiply the size of the geometric modulus with a Modulus Extension Factor (MEF) specific for each sleeve material. Thus, the true modulus becomes $M_t = \text{MEF} \times M_g$.

Alloys and Combinations

Two different alloys for three different feeder combinations were cast in triplicates. The alloys were a pearlitic-ferritic EN-GJS-500-7 and a fully ferritic EN-GJS-450-10 [2]. Both alloys were spheroidal graphite irons (SGI), and their chemical composition is shown in Tab. 1(a). The combination of alloy, sleeve material and feeder modulus can be seen in Tab. 1(b). The castings are identified by alloy (α or β), feeder combination (1, 2 or 3) and triplicate copy (A, B or C). E.g. β3A is EN-GJS-450-10 fully ferritic alloy cast with a combined material feeder sleeve for the top feeder, and no center feeder.

Table A: *Dimension and M_g in mm*

	I	III	IV	V	VI	VII	IX
w	ø32	20	10	30	10	20	ø40
h	40	30	55	50	55	30	60
M_c	7	6	5	9	5	6	8

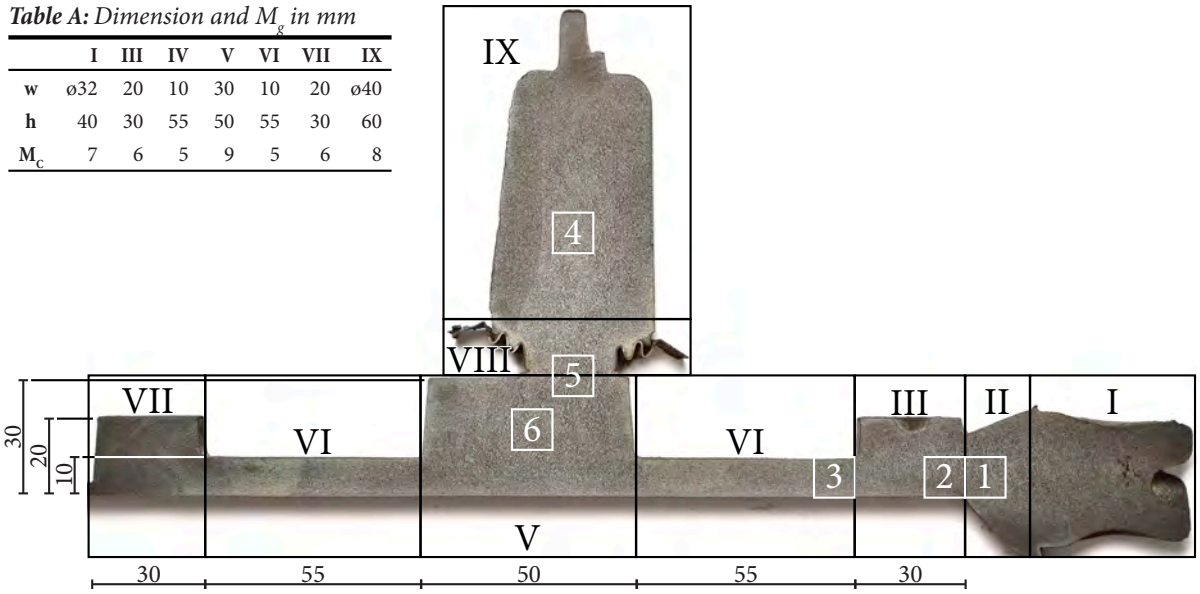

Figure 2: Overview of sectioned casting (α2A). Etched with 1% Nital for 600 s. The casting is divided into 9 non-overlapping areas (Roman numerals) for quantification and analysis of porosities. 6 sections (Arabic numerals) of 10 x 10 mm were cut and color etched. The inserted table (Table A) shows the dimensions and geometric modulus (M_g) of the different areas. All measurements are in mm.

Table 1: Alloy compositions and feeder combinations used.

(a) Alloy compositions in wt%. α is the EN-GJS-500-7 pearlitic-ferritic alloy, and β is the EN-GJS-450-10 fully ferritic alloy.

	CE	C	Si	Mn	P	S	Mg	Cu
α	4.6	3.69	2.75	0.50	0.015	0.005	0.044	0.25
β	4.5	3.35	3.48	0.34	0.017	0.003	0.046	0.10

(b) Sleeve materials: Exothermic (Exo), insulating (Ins) or combined (E/I). Parenthesis shows the true modulus (M_t) in mm.

	α1	α2	α3	β1	β2	β3
Top	E/I (10)	Ins (9)	E/I (10)	E/I (10)	Ins (9)	E/I (10)
Center	Exo (12)	Ins (11)	-	Exo (12)	Ins (11)	-

Production

α1 and α2 was cast at $(1401 \pm 5)\,°C$, α3 was cast at $(1408 \pm 5)\,°C$ and the β-series was cast at $(1392 \pm 5)\,°C$. The poured weight was 8 kg with a pouring time of 3.5 s and a casting weigh of 4 kg. All castings were made on the same vertical molding line. For more details please refer to [1].

Methods

Liquid Penetrant Test

The porosities in the sectioned castings were examined using liquid penetrant testing and classified accordig to the European Standard EN 1370-1:2011 [3]. The analysis of each casting was divided into 9 areas as seen on Fig. 1, and was evaluated for size and type of porosities. The process in fully described here [1].

Deformation Measurements

The deformation of the reverse side of the castings is in this paper described by its flatness value (f_v). In simple terms the f_v is the difference between the highest and lowest point on the surface. The f_v was measured using a Ziess OMC 850 mechanical Coordinate Measuring Machine (CMM) with a resolution of 0.2 µm. The measurements were made using a 3 mm prob which acted as a mechanical filter with respect to the surface roughness. For more detail see [1].

Etchings

Macro Etching All analyzed discs were sectioned using a cold saw, after which the sectioned piece was ground plane. The newly ground surface was etched for 600 s in a 20 °C 1% Nital solution—99 mL Ethyl alcohol and 1 mL Nitric acid (HNO_3). After etching the sectioned casting was cleaned in ethanol and left to dry in a hot air oven at 110 °C for 1800 s. The macro etched castings were analyzed using a magnifying glass—see Fig. 1.

Color Etching The cut out sections (1-6) from castings α1, α2 and β1 was color etched with a picric acid—50 ml Distilled water, 10 g Sodium hydroxide (NaOH), 40 g Potassium hydroxide (KOH) and 10 g Picric Acid ($C_6H_3N_3O_7$). After mixing the mounted and polished pieces were etched at 105 °C. Most pieces required an etching time around 330 s, but some required more. Each piece was analyzed in an optical microscope after etching, and then etching again if the etching was not fully developed.

Results

Porosities

For all 18 castings areas II, IV, VI and VII display no sign of porosities in any of the casting. Area II is the feeder neck of the top feeder, and areas IV and VI are the thin walled sections between the outer ring and the center boss. Area VII is the ring section at the bottom of the casting. Areas I and IX are the feeders and are excluded from the porosity analysis. Thus, the analysis focus on the remaining three areas—III, V and VIII—and the results are shown in Tab. 2.

All 6 castings that used the exothermic sleeves (α1 and β1) displayed no porosities in the areas analyzed. Of the three castings with insulating sleeves and the EN-GJS-500-7 alloy, the α2B showed the smallest category of non-linear isolated porosities (SP1). The same feeder configuration with the fully ferritic EN-GJS-450-10 alloy showed SP1 porosities in 2 of 3 feeder necks (VIII), a single more severe SP2 porosity at the boss (V) and a single SP1 porosity at the upper ring (III). The reference castings without center feeder all displayed porosity defects at the boss (V).

Casting Flatness

All 18 castings have a flatness value (f_v) between 0.33 and 0.50 mm. The results are shown in Tab. 2, displaying each casting configuration as separate bar graphs. The

Table 2: Feeder types and modules are shown in red, orange and yellow boxes. Soundness of individual castings is shown in the bottom section. Green means no porosities. SP indicate non-linear isolated porosities and CP indicate non-linear clustered porosities. The suffix indicate severity—higher is more severe [3]. The graph show the f_v of the different casting groups.

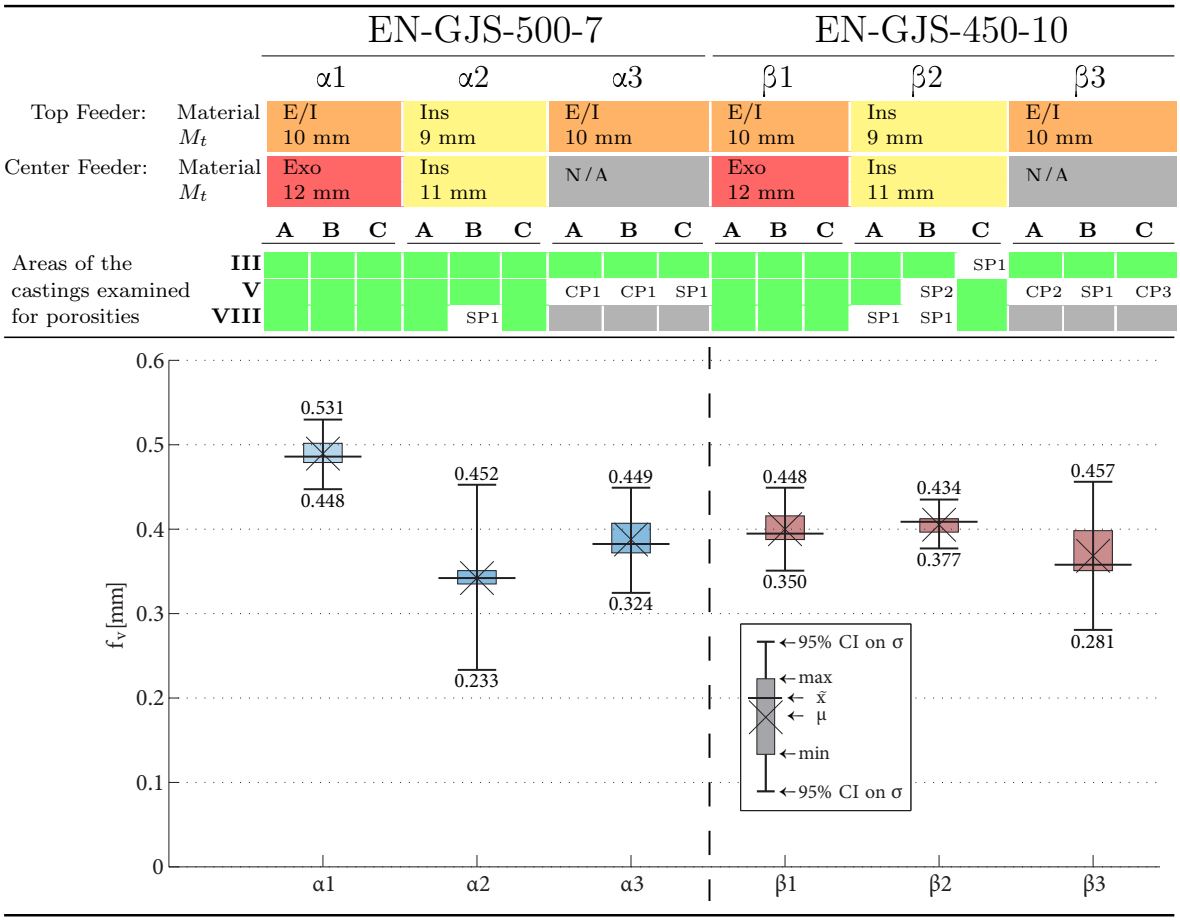

bar ends show the highest and lowest value measured. × mark the arithmetic mean of the population, and — mark the median value. The error bars mark a 95% confidence interval assuming a Gaussian distribution. Using an outliers factor of 3, no outliers were found. There was a greater variation in the pearlitic-ferritic α-alloy, compared to the fully ferritic β-alloy, but only α1 and β2 can be identified as statistically different. All other groups have overlapping confidence intervals and cannot be concluded to be different.

Etchings

Macro Etchings The macro etching had little or no effect on the fully ferritic β-alloy. The lack of reaction showed that these castings contained very little or no pearlite. The analysis of the pearlitic-ferritic α-alloy showed evenly distributed pearlite in all areas of the castings. Dendrite structures were visible to the naked eye in areas I, II, III, V, VIII and IX. Areas IV, VI and VII do not have visible dendritic structures. All α-castings showed clear signs of directional dendrite growth across areas I, II and III. The dendrites

in areas V, VIII and IX did not show a clear direction of solidification. α2A after etching with Nital can be seen in Fig. 1.

Color Etchings Comparing the microstructures of the α- and β-alloys it was seen that the β-alloy display a greater nodule count. All three castings displayed good nodularity in all of the etched sections. The thin walled section (3) showed directional solidification from the edge and towards the center of the section. Dendrites were found in sections 3, 4, 5 and 6 for all three castings. Dendrites were not identified in etchings of section 1 and 2.

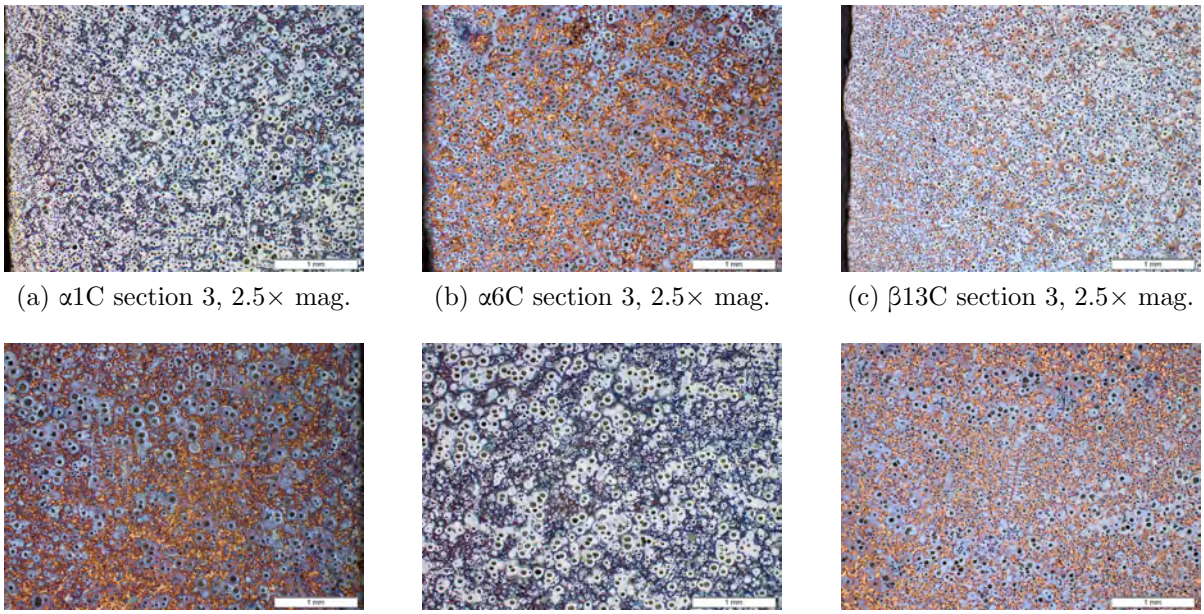

(a) α1C section 3, 2.5× mag. (b) α6C section 3, 2.5× mag. (c) β13C section 3, 2.5× mag.

(d) α1C section 6, 2.5× mag. (e) α6C section 6, 2.5× mag. (f) β13C section 6, 2.5× mag.

Figure 3: Color etchings: Si segregation gives a blue tint. Brown areas are low Si regions.

α1C and β1C with the exothermic sleeves contained a large fraction of low Si eutectic segregation in section 6. α2C with the insulating sleeves, showed a large fraction of low Si eutectic segregation in sections 3, 4 and 5. Furthermore, sections 4 and 5 for castings α1C and β1C showed alignment of the graphite nodules according to the dendritic structure, while the same section for α2C was less orderly and displayed a larger fraction of non-linearized nodules. For section 6 none of the three castings showed a high degree of linearized nodules.

Discussion

Porosities and Deformation

First of all the results show that the test casting could not be cast porosity free without the center feeder. All six castings from α3 and β3 displayed porosities at the boss (V). The porosity analysis also showed that the β-alloy was more prone to porosities, as also the β2 configuration displayed porosities in the boss (V), the top ring (III) and on two

occasions at the feeder neck (VIII) close to the boss. In comparison the α2 castings that had the same feeder configuration showed only a single porosity defect, namely at the feeder neck (VIII). Porosities in the feeder neck do not deem the casting itself unsound, but it indicates that the given feeder is close to the limit of how much it can feed. For both the α- and the β-alloy the feeder configuration using exothermic sleeves showed no sign of porosities at the examined areas.

There were no direct correlation between the flatness value f_v of the castings and the porosities. Comparing the two alloys it was shown that the pearlitic-ferritic α-alloy displayed a greater variance than the fully ferritic β-alloy. The higher Si content of the β-alloy increase the austenite to ferrite transformation temperature [4], which result in an earlier graphite expansion, which again occur at a time where the casting has regained less strength compared with the low Si α-alloy. The pattern plate was measured to have a f_v of 16.4 µm—approx. 20-30 times smaller than the flatness measured on the castings and is thus concluded to have no significant influence on the results.

Solidification and Microstructure

The greater nodule count in the β-alloy cannot be contributed to the difference in alloying elements. Increased Mn content can increase the nodule count, but the β-alloy have a lower Mn content than the α-alloy, and should thus have a lower nodule count. However, the two alloys were cast at different dates and the inoculation procedure may have changed in between. The castings with the exothermic sleeves (α1C and β1C) both showed a large fraction of low Si eutectic solidifying in between the nodules at the boss (6). The insulating sleeves showed the opposite effect, having low Si eutectic at the feeder neck and in the feeder it self. Before making final conclusions in this matter, further color etchings should be made. The etchings are very sensitive with respect to etching time, and the lack of brown areas in section 6 of β6C may be due to under etching. Assuming the etchings are reliable, the phenomena may be explained by the delayed graphite expansion of the exothermic feeders. The boss section (V) will have expanded and pushed out a portion of the low Si eutectic, after which the graphite expansion in the feeder (IX) will push back the last to freeze melt—the low Si eutectic.

The greater tendency to shrink found in the β-alloy may be, in part, related to an improved inoculation procedure, as has previously been shown in gray cast iron [5]. While under-inoculation will result in a decreased graphite expansion, over-inoculation can advance the occurrence of the graphite expansion resulting in a decreased expansion later in the process. Another phenomena that influence the movement of the last to freeze melt through the mushy zone is the thermal center. The movement of the thermal center during solidification—a so called migrating hot spot—has been shown to play a significant role in the development and location of porosities [5, 6]. A migrating hot spot can also be part of the explanation for the different locations of the last to freeze melt, as the not only the different M_t of the different feeders will influence the development and movement of the global and local hot spots, the differences in sleeve material will likewise also influence the migration of the hot spots.

Conclusions

The results showed that the high Si β-alloy was more prone to porosities than the low Si α-alloy, and that the exothermic feeder sleeves could feed both alloys while the insulating sleeves was insuficient for the β-alloy. The measurement of the castings showed that the two alloys had close to the same average f_v, but that the β-alloy displayed a smaller variance. This is suspected to be related to the elevated austinite to ferrite transitions temperature controlled by the Si content. Finally, the color etchings indicated that the low Si segregation of the last to freeze melt were located differently in the castings with exothermic feeders, as compared to the castings with insulating feeders. It is suspected that this is related to the shift in graphite expansion due to the changed M_t and the effect of the migrating hot spot.

Acknowledgments

This work is funded by the PSO funds from the Danish Government, and is performed in collaboration with FOSECO Ltd., MAGMA GmbH, DISA Industries A/S, Vald. Birn A/S and the Technical University of Denmark, Department of Mechanical Engineering. A special thanks to Professor Attila Diószegi and Sadaf Vazehrad at Jönköping University, School of Engineering, Sweden, for their kind assistance with color etching the cut sections.

References

[1] N. K. Vedel-Smith, et al. Quantification of Feeding Effects of Spot Feeding Ductile Iron Castings made in Vertically Parted Molds. *AFS Proceedings*, (1310), 2013.

[2] EN 1563:2012-3—Founding: Spheroidal Graphite Cast Irons, 2012.

[3] EN 1371-1:2011—Founding: Liquid Penetrant Testing—Sand, Gravity Die, and Low Pressure Die Castings, 2011.

[4] Ductile Iron Data. *Ductile Iron Data - for Design Engineers*. Rio Tinto Iron & Titanium Inc., 1990.

[5] Lennart Elmquist, et al. On the Formation of Shrinkage in Grey Iron Castings. *Key Engineering Materials*, 457:416–421, 2011.

[6] Lennart Elmquist and Attila Diószegi. Shrinkage Porosity and its Relation to Solidification Structure of Grey Cast Iron Parts. *International Journal of Cast Metals Research*, 23(1):44–50, 2010.